Epitaxial Science of GaN: Nanowires, Quantum Dots, and Mesoscopic Morphology

Q. Sun,[a] C. D. Yerino,[a] B. Leung, [a] and J. Han*[a]
[a]Department of Electrical Engineering, Yale University, New Haven, CT 06520
*email jung.han@yale.edu

ABSTRACT

In addition to future applications in electronics, optoelectronics, and biophotonics, synthesis of nanostructures such as nanowires, nanorods, and quantum dots offer insights regarding the governing principle of crystal growth that can be applied to a wide range of mesoscopic phenomena. The basis for understanding the morphology of GaN nanosystems during epitaxy is the (kinetic) Wulff theorem which incorporates the concept of energy minimization into a set of geometrical rules depicting shape evolution. An appreciation of the Wulff plot for GaN, a three-dimensional diagram (*v*-plot) where the radial distance is proportional to the growth velocity along that direction, not only assists the interpretation but also facilitates a detailed control of nanoepitaxial processes. To map out the kinetic Wulff diagram, we carried out selective-area growth (SAG) of GaN on polar, nonpolar, and semipolar surfaces under a wide range of conditions (temperature, pressure, and V/III ratio). Salient features on the kinetic Wulff plot include cusps, saddle points, and apexes, which all have implications in shaping the nano-objects. Examples will be given to illustrate the utility of Wulff plots in explaining the topography of nanorods and quantum dots and in aiding a rational design of GaN nonpolar and semipolar growth for solid state lighting applications.

Keywords: Epitaxy, quantum dots, nanowires, nucleation, Wulff, nonpolar, semipolar

1. INTRODUCTION

Gallium nitride has emerged to be one of the most important semiconductor materials during the past two decades for optoelectronic and electronic applications. Since the late 1990s there have been parallel growing interests in the epitaxial formation and exploitation of GaN nanostructures such as quantum dots (QDs) [1, 2], nanowires [3, 4, 5], nanocolumns [6], and confined growth of nanorods [7, 8]. In an attempt to achieve epitaxial alignment of nanowires [4] using GaN mesas prepared by selective area growth (SAG), it became evident to us that both nanoscale synthesis and mesoscopic growth, including the formation of SAG islands and heteroepitaxial dynamics, are governed by the same principle of minimization of surface (and strain) energy, often referred to as Wulff's theorem [9]. The application of the Wulff (or kinetic Wulff) theorem offers a framework to understand a broad range of nano- and mesoscopic epitaxial phenomena, *provided that a concrete knowledge of the Wulff diagram (γ- or v-plots) for the material system, in this case GaN, is available*. In this paper we summaize our attempt to construct the kinetic Wulff plots (*v*-plots) for GaN under different growth conditions over a wide crystallographic orientations. We also provide examples to illustrate how the *v*-plots facilitate understanding and enable rational design of mesoscopic epitaxial processes.

2. BACKGROUND OF KINETIC WULFF THEOREM

2.1 Basic principle

It is generally accepted that the shape and morphology of a growing crystal at mesoscopic scale (between a few nanometers to tens of micrometers) can be adequately described by the so-called Wulff theorem [10]. Wulff theorem was proposed as a solution to the problem of minimizing total surface energy in an anisotropic system under the constraint of mass conservation. In a seminal work by Herring [11], it was shown that the shape of growing crystal can be determined by a procedure known as Wulff construction. A hypothetical 3D Wulff plot of surface energy in polar coordinates (also known as $\gamma(\theta, \phi)$ plot or γ-plot) of simple cubic structure is illustrated in Fig 1 [12].The procedure in deriving the equilibrium polyhedral crystal shape involves the constructing of a plane *perpendicular* to the radius vector at that point. Then the volume which can be reached from the origin without crossing any of the dotted lines will be geometrically similar to the ultimate equilibrium shape for the crystal. The 3D γ-plot predicts an equilibrium shape of

Nanoepitaxy: Homo- and Heterogeneous Synthesis, Characterization, and Device Integration of Nanomaterials, edited by M. Saif Islam, A. Alec Talin, Stephen D. Hersee, Proc. of SPIE
Vol. 7406, 74060L · © 2009 SPIE · CCC code: 0277-786X/09/$18 · doi: 10.1117/12.829140

crystal to be a cube in dashed line based on Wulff construction. For the simple model, one can readily correlate features on the 3D Wulff plot, such as cusps, valleys, and apexes with real-space crystal features such as planes, edges, and corners, respectively. In non-equilibrium thin-film growth and epitaxy, the concept of Wulff construction can be extended with the use of *kinetic Wulff plot (v-plot)* [13] provided that the surface free energy function, $\gamma(\theta, \phi)$, in a traditional Wulff plot is substituted by a semi-empirical function, $v(\theta, \phi)$, where $v(\theta, \phi)$ is the kinetic growth rate of a plane with a surface normal defined by polar (θ) and azimuthal (ϕ) angles [14]. The pairing between features on $v(\theta, \phi)$-plots and kinetic observations remain consistent; the slow growing surfaces (cusps on $v(\theta, \phi)$ plots) tend to expand and dominate while the fast growing surfaces (apexes) will grow to extinction into corners.

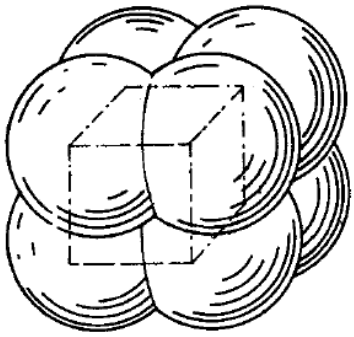

Fig 1. A $\gamma(\theta,\phi)$ plot of a cubic crystal [13].

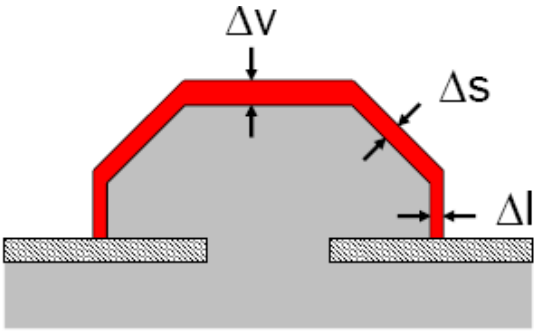

Fig 2 Schematic drawing of a GaN mesa with two SAG growths. Δ**v**, Δ**s**, and Δ**l** denote the incremental thickness along vertical, side, and lateral directions.

2.2 Differential SAG approach

To construct 3D $v(\theta, \phi)$ plots as the basis for understanding and tailoring GaN growth designs, we carried out SAG experiments concurrently on different crystallographic planes including *c*-plane (Ga- and N-polar), *a*-plane, *m*-plane, and the semipolar (11$\underline{2}$2) plane so a sufficiently large span in polar and azimuthal angles is covered. Growth rates measured from SAG mesas on different planes are normalized for consistency; SAG mesas of identical fill factors are used. We note that our study differs from earlier SAG study [15] in which the linear dimension from the edge of mask to a surface of interest is taken to establish average growth rate. In our study, differential selective area growth (Δ-SAG) with consecutive SAG experiments was performed, as illustrated in Fig 2. By comparing the dimensions of the mesa before and after the 2nd SAG growth, one can measure the differential lengths (Δ**v**, Δ**s**, and Δ**l**) and produce a kinetic Wulff plot (*v*-polt).

To facilitate access to more crystallographic planes, we design SAG masks with annular ring patterns to induce concave growth fronts in the inner ring. The presence of concave facets in the in-plane directions helps to promote and stabilize fast-growing planes according to Borgstrom principle [16, 17]. In the category of *concave* growth, which is ubiquitous in island coalescence stage, the fast growing planes will expand its surface area while the slow ones will be reduced to extinction.

2.3 Three-dimensional mapping of *v*-plot for GaN

Figure 3 shows a 3D *v*-plot, viewing along <10$\underline{1}$1> and <11$\underline{2}$2> directions, for a growth condition of 1070°C, 100 mbar, and a V/III ratio of 250. False-colored image from red to blue is used to depict the measured (or interpolated) growth rates from the slowest to the fastest. We have identified cusp points (local minima) at [0001], <10$\underline{1}$1>, <11$\underline{2}$0>, <10$\underline{1}$0>, and [000$\underline{1}$]. These directions (or planes normal to the directions), arranged in increasing order of their respective polar angles (θ) relative to the [0001] axis, are responsible in defining the shape of nucleation islands, quantum dots, and nanocrystals having convex curvature on mesoscopic scale. In addition to plotting the positions of cusps in Fig 3, we also include measured saddle points produced by concave growth fronts in annular rings. The identified saddle points

are along the following directions: [11$\underline{2}$2], [10$\underline{1}$2], and [101$\underline{n}$] (vicinal to [10$\underline{1}$1], *i.e.* $n \sim 1$). The presence of these saddle points can be verified by studying annular-ring SAG patterns on *a*-plane GaN [9].

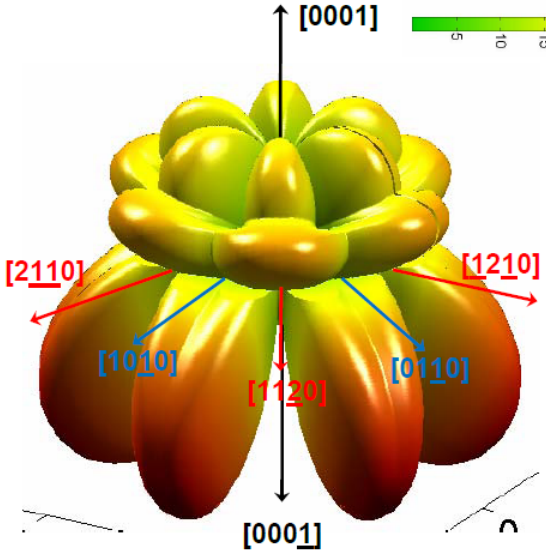

Fig 3. 3D *v*-plot for GaN grown at 1070 ºC, 100 mbar, V/III: 250.

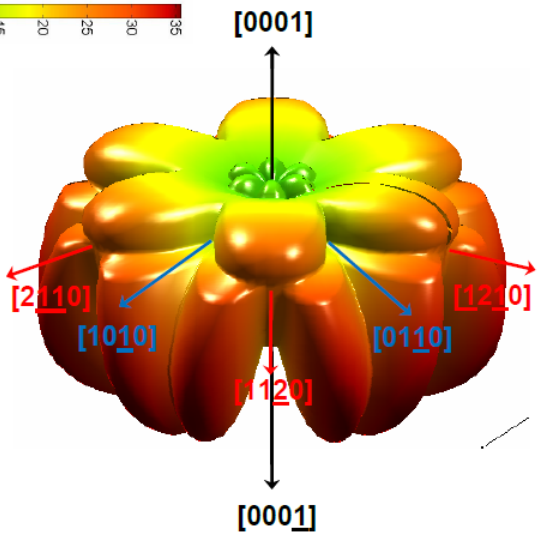

Fig 4. 3D *v*-plot for GaN grown at 1000 ºC, 300 mbar, V/III: 500

As was implied by previous works of epitaxial lateral overgrowth [18], the growth rates along different directions depend strongly on the local stoichiometry. We have performed concurrent Δ-SAG experiments under a condition of much higher equivalent V/III ratio [9]. In this case the relative growth rates of nearly all Ga-polar planes (represented as the "northern hemisphere", $0<\theta<\pi/2$) on the 3D *v*-plot in Figure 4 is suppressed. Furthermore, the "waist" of the 3D *v*-plot, pertaining to growth rates of nonpolar planes, is increased considerably with the *a*-plane much faster than the *m*-plane in growth rate. These two examples serve to illustrate the variability in Wulff plots under standard GaN MOCVD conditions. The *v*-plot can therefore be considered as useful fingerprints of particular conditions that enable trans-platform correlation of growth experiments. It is conceivable that growth practices such as flow modulation, co-doping, and morphactant use could impact *v*-plot substantially. Efforts in surveying and documenting these practices are currently underway. A comprehensive knowledge of the variance of *v*-plot will pave the way for a detailed control of heteroepitaxial dynamics when different *v*-plots are rationally combined and permutated.

3. NANO-EPITAXY

3.1 Quantum Dots Growth

Epitaxy of GaN quantum dots based on S-K growth mode has been reported with both molecular beam epitaxy (MBE) [1] and MOCVD [2]. In a manner similar to the study of InAs QDs on GaAs, the formation of GaN QDs on AlN was explored by tuning the standard growth parameters such as V/III ratio, temperature, and the thickness of GaN layers. Assuming that adatom diffusion is sufficiently high so that near equilibrium conditions are approached at nano- or meso-scopic scale, the energetics describing the three-dimensional (3D) formation of QDs has been analyzed in terms of the change of free energy [19]

$$\Delta F = -\Delta\mu V + \sum_{i\neq AB}\gamma_i S_i + S_{AB}(\gamma_A - \beta) + \varepsilon_0 m^2 VR \qquad (1)$$

where $\Delta\mu$ is the supersaturation, V is the volume of the QD, γ_i and S_i are the surface energy and area of the *i*-th facet. S_{AB} is the contact area, γ_A is the surface energy of the basal face of A before adhesion onto substrate B. β is the adhesion energy and is related to the interfacial energy γ_{AB} through the equation $\gamma_{AB} = \gamma_A + \gamma_B - \beta$. m is the epitaxial misfit, ε_0 is the elastic constant of QD, and R is the relaxation energy factor ($0<R<1$) depending on the degree of (elastic and plastic) relaxation. One can determine the equilibrium shape of QDs when the derivative of Eq (1) is zero at constant volume, which leads to the following two expressions Eq (2a-b) consisting of n_i equations; Eq 2a is valid for *i*=A, and AB, and Eq 2b applies to all other facets.

$$\frac{\Delta\mu - \varepsilon_0 m^2 R}{2} = \frac{\gamma_i - \gamma_A \cos\theta_i + \varepsilon_0 m^2 \dfrac{V}{n_i}\dfrac{\partial R}{\partial S_i}\Big|_{AB}}{h_i - h_A \cos\theta}. \tag{2a}$$

$$\frac{\Delta\mu - \varepsilon_0 m^2 R}{2} = \frac{2\gamma_A - \beta + \varepsilon_0 m^2 V \dfrac{\partial R}{\partial S_{AB}}\Big|_i}{H}. \tag{2b}$$

Equations 2a-b (generalized Wulff-Kaishew theorem) provide an analytical link between experimentally observed QDs, especially its detailed shape, and Wulff diagram such as the ones shown in Fig 3-4, where γ_i correspond to minimums or cusps on a kinetic Wulff plot. Such an approach was taken to describe GaN quantum dots with pyramidal (10$\underline{1}$3) facets [20].

3.2 Nanowires by VLS method, confined nanoepitaxy

The basic principle of vapor-liquid-solid (VLS) mechanism for anisotropic growth of 1D nanostructures was summarized by Wagner.[21] Prerequisites that were identified include: (1) A sizable disparity in reaction kinetics between regular vapor-solid (VS) and the VLS mechanisms, thus mandating a low supersaturation for growth selectivity; (2) the creation and retention of liquid droplets to facilitate adsorption and incorporation of vapor phase species; and (3) the need to have nucleation sites with appropriate crystallographic orientations conducive to the minimization of surface energies. Criterion (1) helps to elucidate the popularity and success in the synthesis of GaN nanowires through hot-wall, flow-tube furnace chamber in which elemental Ga source is placed upstream of catalyst-treated substrates.[22] The proximity of a desorptive source to an adjacent growth surface spontaneously creates an ambient that is close to thermodynamic equilibrium. Favorable conditions for nanowire growth (under low supersaturation) is empirically derived by adjusting the relative positioning between the Ga boat and substrate due to spatial gradients in temperature and Ga flux. On the other hand, modern MOCVD involves a much different and complex process in which organometallic precursors (undersaturated even at room temperature) are transported in vapor phase with minimum dissociation to the vicinity of growth surface. The precursors then undergo rapid pyrolysis decomposition upon entering the heated zone near surface (thermal boundary layer), creating a highly inhomogeneous profile and a mass-transport limited growth process.[23]

We have reported previously the growth of AlGaN nanowires by MOCVD.[24] In the synthesis of nanowires using non-equilibrium, epitaxial techniques such as MOCVD and MBE, surface kinetics including adatom diffusion need to be taken into consideration. [25] It was shown recently [26] with chemical beam epitaxy (CBE) that growth of InAs nanowires takes place primarily through mass transport of In adatoms within the radius of diffusion length and incorporation preferentially at catalyst tips. In non-equilibrium synthesis of AlGaN nanowires by MOCVD, presence of both Al and Ga adatoms as well a large difference in bond strength and consequently diffusion mobility [27] create a unique interplay between kinetic and thermodynamic processes.

High-resolution TEM reveals the presence of well-defined crystallographic planes at the nanowire tips (Fig. 5a). Crystallographic analysis indicates that the inclined droplet/nanowire interface (62° to growth direction) corresponds to a pyramidal {10$\underline{1}$1} plane, a plane likely to have the lowest surface energy or growth rate during MOCVD growth [28] Based on the electron diffraction data, crystallographic symmetry consideration, and reported works of ELO, a three-dimensional rendition of the tip structure is given in Fig. 5b. A well-known phenomenon in nanoscale nucleation, based on Wulff theorem, is that a rapidly growing surface (or a facet with high surface energy) tends to grow itself out of

existence. Our consideration of surface energetics (Fig 5b), on the contrary, leads to an intriguing if not paradoxical distinction for nanowire growth in which selective and preferential growth, *mediated by the presence of catalyst and/or liquid droplets,* takes place at and is confined to a surface/interface with a low surface energy [29], thus affording a self-sustaining process for anisotropic growth.

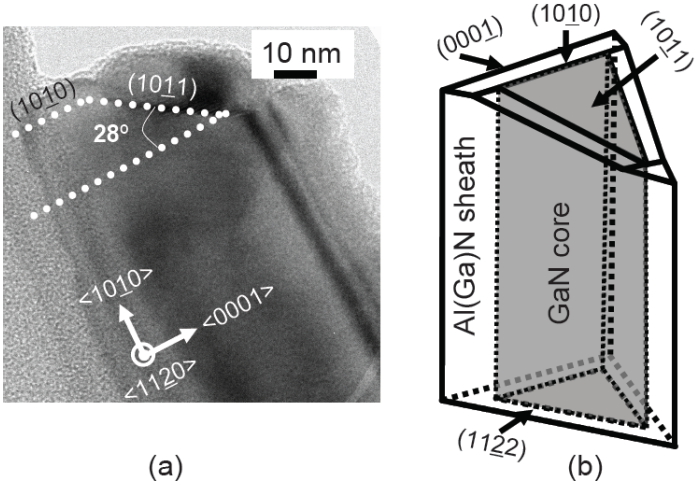

Fig 5. (a) High-resolution TEM image of AlGaN (x, Al-gas = 50%) nanowire near the tip region, the nanowire growth direction is along <1010>, it is viewed along the <1120> direction, with a very small degree of tilting toward <0001> or <0001> direction, (b) 3D diagram of the nanowire tip, the triangular cross section is bound by two {1122} planes and basal (0001) plane, the droplet is on the tilted (1011) plane.

As we analyze the confined nanoepitaxy (CNE) in forming one-dimensional (1D) like nanorods through the use of nanopatterned dielectric masks, it becomes clear that CNE proceeds in two stages: (1) An initial filling-up stage where adatoms are funneled selectively into nanoholes, the shape of the nanorods conforms to the geometric boundary defined by the dielectric holes, and (2) an out-growth stage, where GaN crystal emerges from the nanoholes and proceeds with no physical constraints. Stage (2) is completely governed by the Wulff (or kinetic) principle with {10$\bar{1}$1} planes dominating all the c-plane growth.

4. MESOSCOPIC MORPHOLOGY

An important class of mesoscopic phenomenon is the dynamics of heteroepitaxy. Epitaxial growth on highly mismatched substrates can be divided into four stages, including (i) three-dimensional nucleation, (ii) growth of isolated islands, (iii) coalescence of islands, and (iv) completion of coalescence and transition to steady-state morphology. Step (i) occurs at the atomistic scale and is affected by a complex set of parameters such as elastic strain, surface energy disparity, valence mismatch, density of steps, surface reconstructions, and surface kinetics. Nucleation has been treated at the atomistic scale both analytically and numerically [30]. Except for a handful of model systems (Si/Ge and InAs/GaAs) with strong coupling between modeling and experimental finding, the technological solution to nucleation is attained typically through empirical approaches and is not addressed in the current study. The growth dynamics of stages (ii) and (iii) is treated analytically and often qualitatively based on grain growth [31] and orientation selection, [32] primarily using isotropic assumptions of kinetics and thermodynamics. Microstructure and morphology of the eventual thin films are developed and established in stages (ii) and (iii) with only minor changes in stage (iv).

For growth of GaN on *c*-plane sapphire, a working (in fact groundbreaking) procedure directing the heteroepitaxial evolution in stages (i)-(iv) was pioneered by Akasaki et al [33]. A qualitative model was proposed subsequently [34]. However, the literature regarding nonpolar planes such as *m*-plane, *a*-plane, and the semipolar planes shows a diverse range of growth procedures and results with no clear correlation. We demonstrate in this work that the knowledge of kinetic Wulff plot (or *v*-plot) enables the interpretation of stages (ii)-(iv) at a detailed, mesoscopic level. An accurate mapping of Wulff plots for MOCVD growth of GaN over the entire three-dimensional (3D) crystallographic space is presented for the first time. While the Wulff plot concept has been largely confined to introductory textbooks, we

provide examples of varying complexity to illustrate its value in interpreting semipolar/nonpolar growth dynamics and, ultimately, in facilitating a rational control of heteroepitaxial process.

4.1 Semipolar GaN islands

Turning to the application of Wulff plots, we first focus on the morphology of nucleation islands. Given that all the surfaces involved are of convex nature, the cusps on the 3D *v*-plot will determine the final appearance. The shape of nucleation islands occupies a central role in deciding the microstructural quality of a heteroepitaxial layer. It has been shown that nucleation islands with inclined facets could facilitate the bending of threading dislocations [35, 36] and partial dislocations [37], thus enhancing the possibility of defect interaction and annihilation. To apply the *v*-plot to a less obvious example with high anisotropy, we considered the morphology of islands associated with the semipolar (11$\underline{2}$2) plane. Fig 6 shows SEM images of two SAG islands on semipolar (11$\underline{2}$2) surface under different stoichiometry of V/III abundance. On the left we have a relatively Ga-rich condition. The shape of the SAG mesa can be completely interpreted by the *v*-plot in Fig 3, now rotated about 58° to align the surface normal with the semipolar axis. The blue circle high lights the *a*-plane (11$\underline{2}$0) which is relatively stable due to a low growth rate (corresponding to a narrow waist for the *v*-plot on the left). The green circle on the *v*-plot indicates the measured semipolar growth rate, which is relatively high and becomes extinct in convex growth. By increasing the V/III ratio, we are able to slow down the growth rates of most of the Ga-polar planes (indicated by the "shrinking" of the "northern hemisphere" in the *v*-plot on right), especially the semiploar (11$\underline{2}$2) plane labeled by a green circle. Consequently we see the emergence of a relatively flat top on the SAG island. Applying these trends to the growth of (11$\underline{2}$2)-GaN on *m*-sapphire, we found that higher V/III conditions promoted a smooth (11$\underline{2}$2) final surface morphology, while low V/III conditions produced a rough, striated surface, corresponding to a quick decay of the *in situ* reflectance.

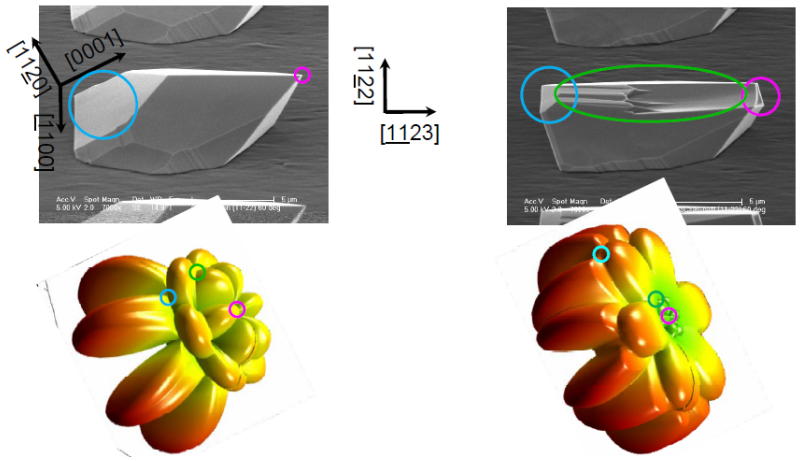

Fig 6. SAG islands grown on (11$\underline{2}$2) semipolar GaN, grown at conditions corresponding to *v*-plots in Fig 3 (left) and Fig 4 (right), respectively. Colored circles show relationship between SAG facets and points on the *v*-plots.

4.2 Island coalescence

Island coalescence in its simplest form can be considered as the interaction of two facets intersecting with a concave angle [13]. In the realistic 3D situation, we propose that the following procedure be applied to the 3D *v*-plot to deduce the needed information regarding concave growth: (i) Plot the two surface-normal vectors that are associated with the two planes, (ii) slice the 3D *v*-plot with the plane defined by the two vectors in (i), (iii) the section of the *v*-plot within (or in the vicinity of) the 2D slice provides the information of growth rates between the two surface-normal directions, and (iv) the maximums on the 2D contour (and the contour's vicinity) will define the stable facets under concave growth. In Fig 7 we show the correlation between coalescence dynamics and *v*-plot, especially focusing on the interplay between cusps and saddle points on the *v*-plot. Going beyond the conventional *c*-axis with 6-fold symmetry, we will illustrate the coalescence process with *a*-plane (11$\underline{2}$0) GaN. On the left side of Fig 7, from top to bottom, shows the coalescence of two (10$\underline{1}$1) facets along the [10$\underline{1}$0] direction (*m*-axis). The two original (10$\underline{1}$1) facets, labeled on the *v*-

plot by two light blue arrows, forms a *concave* front along the m-axis (red arc arrow in the upper left SEM image) and at the same time a *convex* front along the c-axis (green arc arrow in the upper left SEM image). Wulff's theorem will therefore require the final stable facet to be a minimum in the polar direction (green curve on the upper half of v-plot in Fig 7) and simultaneously a maximum in the azimuthal direction (red curve on the upper half of v-plot in Fig 7), thus predicting a stable facet of (11$\underline{2}$2), in good agreement with the experimental observation (lower left SEM image). Similarly, we consider the coalescence of islands along *c*-axis, between the pyramidal (10$\underline{1}$1) and the N-polar (000$\underline{1}$) planes (right side of Fig 7). The two original planes dictate that the resultant new planes to be a saddle point of the character of pyramidal *m*-plane on the "southern hemisphere" of *v*-plot (N-polar), with the only plausible choice to be (10$\underline{1}$2), once again in agreement with the detailed SEM analysis.

In the growth of *a*-plane GaN on *r*-plane sapphire, we have found that the coalescence behaviors in Fig 7 lead to commonly observed pits, bound by both (11$\underline{2}$2) and (10$\underline{1}$2) planes.[9] The presence or absence of these pits is dictated by the relative growth rates of the (11$\underline{2}$2) and (10$\underline{1}$2) planes compared to the (11$\underline{2}$0) *a*-plane. If the (11$\underline{2}$2) and (10$\underline{1}$2) planes are very fast (Fig 6 left) then the pits quickly fill-in and leave a smooth surface, but if the *a*-plane growth rate is similar to or faster than (11$\underline{2}$2) and (10$\underline{1}$2) (Fig 6 right), then pits remain on the surface as the epilayer grows. Furthermore, the entire morphological evolution of nonpolar GaN, from the islanding to the coalescence stage (stages ii-iv), can be modeled based on the Wulff plot, a the results of which will be reported elsewhere.[38]

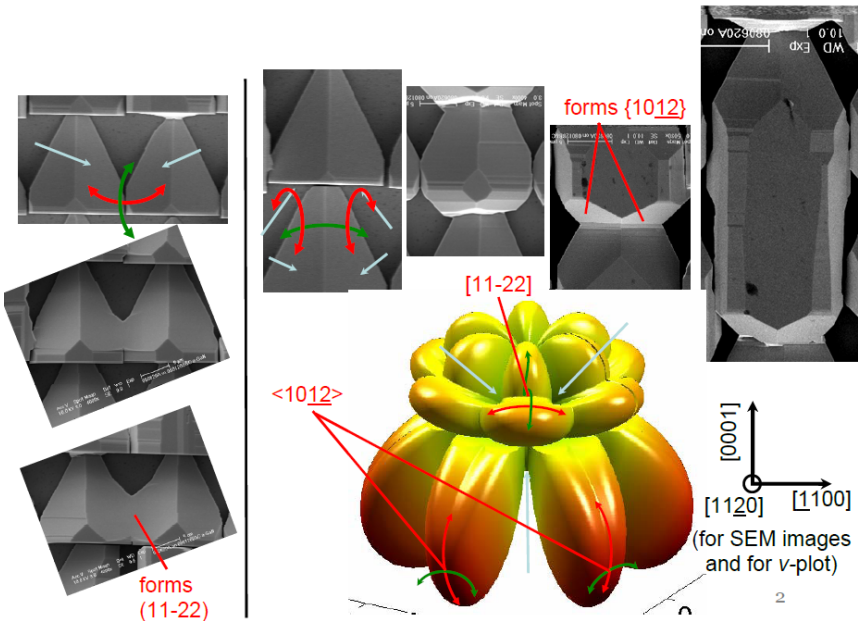

Fig 7. SEM images showing the coalescence process of adjacent SAG islands grown on *a*-plane GaN. Left: coalescence along the [10$\underline{1}$0] direction. Right: coalescence along the [0001] direction. Red and green arcs (SEM images) show concave and convex growth fronts that correspond to maxima and minima on the *v*-plot (red and green arcs on plot), respectively.

5. CONCLUSION

Nano- and mesoscopic heteroepitaxy has been a critical field in enabling contemporary applications in electronics and optoelectronics. The majority of these advances, nevertheless, were brought forth in an empirical way. We are at an initial stage of verifying, establishing, and applying the kinetic Wulff concept to mesoscopic epitaxial processes. A few examples were provided in this paper to illustrate the universality and coherence of this concept. We believe a thorough understanding of this principle will pave the way for tackling complex problems such as heteroepitaxy of nonpolar/semipolar GaN, and nanoscale synthesis.

REFERENCES

[1] F. Widmann, B. Daudin, G. Feuillet, Y. Samson, J. L. Rouviere, N. Pelekanos, J. Appl. Phys., **83**, 7618 (1998).
[2] K. Tachibana, T. Someya, and Y. Arakawa, Appl. Phys. Lett., **74**, 383 (1999).
[3] X. F. Duan, C. M. Lieber, J. Am. Chem. Soc., **122**, 188 (2000).
[4] K. Kim, T. Henry, G. Cui, J. Han, Y. Song, A. V. Nurmikko, H. Tang, Phys. Stat. Sol. (b) 244, 1810-1814 (2007).
[5] G. T. Wang, A. A. Talin, D. J. Werder, J. R. Creighton, E. Lai, R. J. Anderson, and I. Arslan, Nanotechnology, **17**, 5773, (2006).
[6] M. Yoshizawa, A. Kikuchi, M. Mori, N. Fujita and K. Kishino, Jpn. J. Appl. Phys. **36,** L459, (1997).
[7] S. D. Hersee, X. Y. Sun, X. Wang, Nano. Lett., **6**, 1808 (2006).
[8] S. Kim, J. L. Schroeder, and T. D. Sands, J. Cryst. Growth, **310**, 1107 (2008).
[9] Q. Sun, C. D. Yerino, T.-S. Ko, Y. S. Cho, I.-H. Lee, J. Han, and M. E. Coltrin, J. Appl. Phys. **104**, 093523 (2008).
[10] G. Wulff, Z. Kristallogr. **34**, 449 (1901).
[11] C. Herring, Phys. Rev., **82**, 87 (1951).
[12] P. Bennema in Crystal Growth: an Introduction, ed by P. Hartman, p. 342, (1973), North-Holland Publishing, Amsterdam.
[13] D. Du, D. J. Srolovitz, M. E. Coltrin, and C. C. Mitchell, Phys. Rev. Lett. **95**, 155503 (2005).
[14] D. Du and D. J. Srolovitz, J. Crystal Growth, **296**, 86,(2006).
[15] B. Beaumont, S. Haffouz, and P. Gibart, Appl. Phys. Lett. **72**, 921 (1998).
[16] S. H. Jones, L. K. Seidel, K. M. Lau, and M. Harold, J. Cryst. Growth **108**, 73 (1991).
[17] H. Buckley, Crystal Growth (Wiley, New York, 1951) p.125.
[18] H. Marchand, J.P. Ibbetson, P.T. Fini, S. Keller, S.P. DenBaars, J.S. Speck, U.K. Mishra, J. Crystal Growth, **195**, 328, (1998).
[19] P. Muller and R. Kern, Surf. Sci. 457, 229-253 (2001).
[20] N. Gogneau, D. Jalabert, E. Monroy, T. Shibata, M. Tanaka, and B. Daudin, J. Appl. Phys., **94**, 2254 (2003).
[21] R. S. Wagner in Whisker Technology, ed. by A. P. Levitt, p. 47, (1970), John Wiley & Sons, New York.
[22] For example, C. Chen, C. Yeh, C.Chen, M. Yu, H. Liu, J. Wu, K. Chen, L. Chen, J. Peng, and Y Chen, J. Am. Chem. Soc., **123**, 2791 (2001).
[23] G.B. Stringfellow, Mat. Sci. and Eng. B **87**, 97 (2001).
[24] J. Su, M. Gherasimova,G. Cui, H. Tsukamoto, J. Han, T. Onuma, M. Kurimoto, S. F. Chichibu, C. Broadbridge, Y. He, A. V. Nurmikko, Appl. Phys. Lett. **87**, 183108 (2005);
[25] M. Kasu and N. Kobayashi, J. Cryst. Growth **174**, 513 (1997).
[26] L. E. Jensen, M. T. Bjork, S. Jeppesen, A.I. Persson, B.J. Ohlsson, and L. Samuelson, Nano Lett. **4**, 1961 (2004).
[27] M. Gherasimova, G. Cui, Z. Ren, J. Su, X. Wang, J. Han, K. Higashimine, and N. Otsuka, J. Appl. Phys. **95**, 2921 (2004).
[28] K. Hiramatsu, K. Nishiyama, A. Motogaito, H. Miyake, Y. Iyecika, and T. Maeda, Phys. Stat. Sol. A **176**, 535 (1999).
[29] Y. Wu, Y. Cui, L. Huynh, C. J. Barrelet, D.C. Bell, and C.M. Lieber, Nano Lett. **4**, 433 (2004).
[30] J. A. Venables in Thin Films: Heteroepitaxial Systems, ed. by W. K. Liu and M. B. Santos, p. 1, (1999), World Scientific, Singapore.
[31] C. V. Thompson, Annu. Rev. Mater. Sci., **20**, 245, (1990).
[32] A. van der Drift, Philips Res. Repts., **22**, 267, (1967).
[33] H. Amano, I. Akasaki, K. Hiramatsu, N. Kiode, and N. Sawaki, Thin Solid Films, **163**, 415 (1988).
[34] I. Akasaki, H. Amano, Y. Kiode, K. Hiramatsu, and N. Sawaki, J. Cryst. Growth, **98**, 209 (1989).
[35] H. Lahrèche, P. Vennégues, B. Beaumont, P. Gibart. J. Cryst. Growth, **205**, 245 (1999).
[36] D. Hull and D. J. Bacon, Introduction to Dislocations, 4th ed. (Elsevier, Oxford, 2001), Vol. 1, Chap. 4, p. 79.
[37] C. F. Johnston, M. J. Kappers, and C. J. Humphreys, J. Appl. Phys., **105**, 073102 (2009).
[38] C. D. Yerino, Q. Sun, T. S. Ko, Yu Zhang, I.-H. Lee, and J. Han (unpublished).